REUSABLE METALLIC THERMAL PROTECTION SYSTEMS DEVELOPMENT

Max L. Blosser*, Carl J. Martin*, Kamran Daryabeigi*, Carl C. Poteet **

*NASA Langley Research Center, Hampton, VA, USA
** JIAFS, The George Washington University, Hampton, VA, USA

ABSTRACT

Metallic thermal protection systems (TPS) are being developed to help meet the ambitious goals of future reusable launch vehicles. Recent metallic TPS development efforts at NASA Langley Research Center are described. Foil-gage metallic honeycomb coupons, representative of the outer surface of metallic TPS were subjected to low speed impact, hypervelocity impact, rain erosion, and subsequent arcjet exposure. TPS panels were subjected to thermal vacuum, acoustic, and hot gas flow testing. Results of the coupon and panel tests are presented. Experimental and analytical tools are being developed to characterize and improve internal insulations. Masses of metallic TPS and advanced ceramic tile and blanket TPS concepts are compared for a wide range of parameters.

1. INTRODUCTION

Future reusable launch vehicles (RLV's) will require greatly improved thermal protection systems (TPS) to achieve the ambitious goal of reducing the cost of delivering a payload to orbit by an order of magnitude. The large surface area and ambitious mission of a single-stage-to-orbit (SSTO) RLV, such as the VentureStar (Ref. 1) shown in figure 1, require a TPS that is very mass efficient and needs little maintenance. Achieving the rapid turnaround and low life-cycle costs required for a commercial RLV will require drastic improvements over the Space Shuttle TPS, which is estimated to require 40,000 hours of maintenance between typical flights (Ref. 2).

An improved TPS, suitable for RLV's, must not only perform its primary function of maintaining the underlying vehicle structure within acceptable temperature limits, but must also be durable, operable, cost effective, and low mass. Durability implies resistance to damage from such environmental threats as handling, low-speed impact, hypervelocity impact, and rain impact as well as the ability to tolerate some level of damage without requiring repair. Operability includes ease of removal, replacement and repair, and minimal maintenance between flights (e.g., minimize or eliminate waterproofing). Cost effectiveness considerations include initial development, fabrication and installation costs, and maintenance costs over the life of the vehicle as well as the impact of TPS on the vehicle performance. The mass of the TPS and limitations on all-weather flying capability significantly affect the performance of the vehicle.

Figure 1: VentureStar single-stage-to-orbit reusable launch vehicle.

A number of approaches to the daunting task of developing a suitable TPS for future RLV's are being pursued, including improvements to ceramic tiles and blankets, refractory composite heat shields, and metallic TPS. This paper describes metallic TPS development efforts at NASA Langley Research Center (LaRC). Much of the pioneering work on metallic TPS was performed at NASA LaRC. As illustrated in figure 2, concepts progressed from early metallic heat shields (Ref. 3) to titanium multiwall concepts (Ref. 4) to superalloy honeycomb sandwich panels (Ref. 5). Much of this early, NASA-funded work focused on developing metallic TPS as an alternative to the ceramic TPS on Shuttle Orbiters. Titanium multiwall and superalloy honeycomb sandwich panel concepts were conceived at NASA LaRC. The detailed design and fabrication was performed by Rohr, Inc. (now BF Goodrich, Aerostructures Group). The testing and evaluation was performed by NASA LaRC.

More recently, the advent of the X-33 program (Ref. 6), in which a half-scale experimental vehicle will be flown to develop RLV technologies, brought a renewed interest in metallic TPS. Under Phase I of the X-33 program, NASA LaRC entered into a cooperative agreement with McDonnell Douglas Aerospace (now Boeing, Huntington Beach) to develop metallic and refractory composite TPS for an RLV. Much of the metallic TPS related work accomplished under that task is documented in reference 7. Under Phase II of the X-33 program, BF Goodrich, Aerostructures Group, is leading the development of the metallic TPS (Ref. 8) for the X-33 vehicle. NASA LaRC has several tasks with BF

Goodrich to provide analysis and testing of the X-33 metallic TPS.

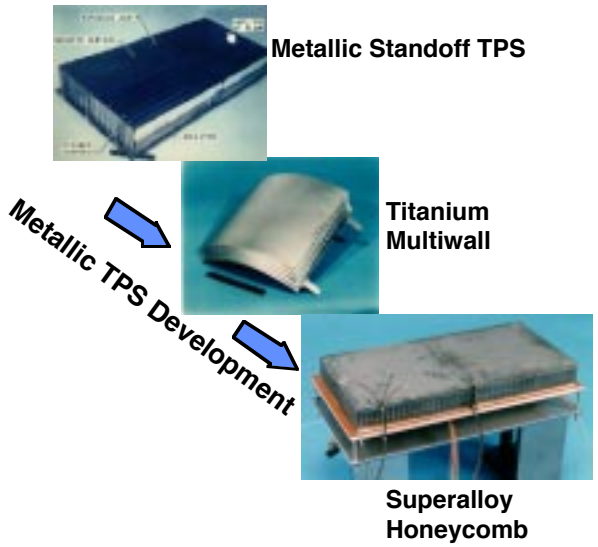

Figure 2: Metallic TPS development at NASA LaRC.

The TPS for RLV's includes different concepts for nose caps, wing leading edges, control surfaces, windward surfaces, and leeward surfaces. The metallic TPS concepts discussed in this paper are primarily applicable to the large windward surfaces of a vehicle.

This paper describes recent efforts at NASA LaRC to develop technologies for metallic TPS. Development efforts include concept development, coupon testing for durability, testing of TPS panel arrays, characterization and improvement of internal insulation, and parametric weight comparisons with competitive TPS concepts.

2. METALLIC TPS CONCEPTS

Metallic TPS use a fundamentally different design approach than ceramic tile and blanket concepts. Ceramic tile and blanket concepts require materials that act as a thermal insulator and also perform the structural functions of maintaining the TPS shape and resisting inertial and aerodynamic loads. Metallic TPS concepts seek to decouple the thermal and structural functions by providing a metallic shell to encapsulate internal insulation, maintain panel shape and support mechanical loads. This decoupling allows the use of structurally efficient materials and configurations as well as thermally efficient internal insulations. Of course, the functions cannot be totally decoupled. The structural connections between the outer surface and substructure must be minimized to reduce heat shorts, and the internal insulation must still resist inertial and acoustic loads (perhaps attenuated by the metallic shell). However, this approach opens up a wide range of possible TPS configurations.

Current metallic TPS concepts use a foil-gage, superalloy honeycomb sandwich to form the hot outer surface. Two different configurations are being pursued. NASA LaRC has been studying a superalloy honeycomb sandwich (SA/HC) TPS (Ref. 7) consisting of lightweight fibrous insulation encapsulated between two honeycomb sandwich panels (figure 3). The panels are designed to be mechanically attached directly to a smooth, continuous substructure. Each panel is vented to local pressure so that aerodynamic pressure loads are carried by the substructure rather than the outer honeycomb sandwich of the TPS. The outer surface is comprised of a foil-gage Inconel 617 honeycomb sandwich and the inner surface is a titanium honeycomb sandwich with part of one facesheet and core removed to save weight. Beaded, foil-gage, Inconel 617 sheets form the sides of the panel to complete the encapsulation of the insulation. The perimeter of the panel rests on a RTV (room temperature vulcanizing adhesive) coated Nomex felt pad that prevents hot gas flow beneath the panels, provides preload to the mechanical fasteners, and helps damp out panel vibrations.

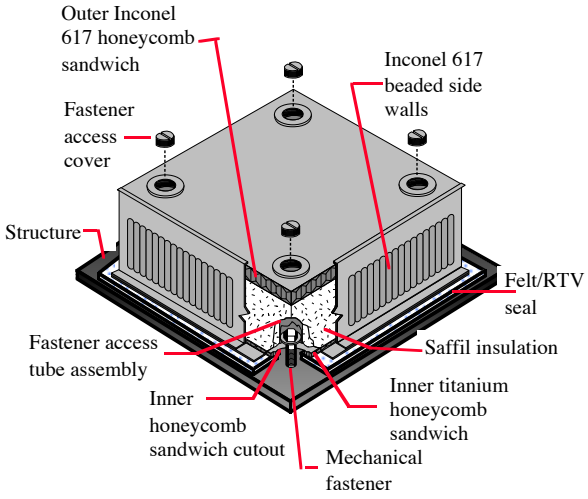

Figure 3: Superalloy honeycomb sandwich (SA/HC) TPS.

BF Goodrich is developing a different configuration (figure 4) using similar materials and fabrication techniques for the X-33 vehicle (Ref. 8). These X-33 metallic TPS panels form an aeroshell which is designed to carry the aerodynamic pressure on the outer surface. Each TPS panel consists of a superalloy honeycomb sandwich heat shield with foil-encapsulated fibrous insulation attached to the inner side. Each square panel is mechanically attached to a metallic, stand-off bracket (rosette) at each corner, and has foil extensions that overlap and seal between the panels. Because the TPS is designed to support the aerodynamic pressure on the outer hot surface, the panel-to-panel seals must carry the aerodynamic pressures and prevent hot gas ingress between adjacent panels to avoid damage to the underlying structure.

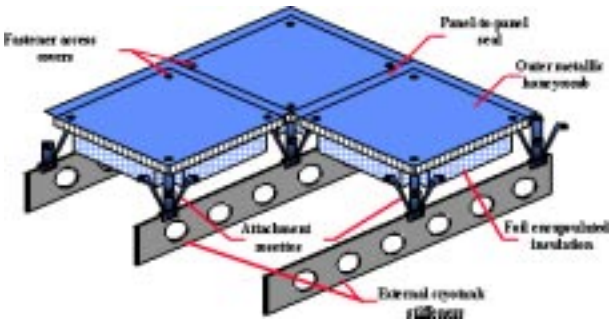

Figure 4: X-33 metallic TPS.

Both metallic TPS configurations have advantages and disadvantages. The X-33 TPS (figure 4) has larger panels that should be simpler and less expensive to fabricate. Deformations of the outer surface due to thermal expansion and bowing are well isolated from the substructure. The constant height stand-off brackets provide a fixed offset from the vehicle structure, and varying the insulation thickness is simple to accomplish. However, carrying the aerodynamic pressure on the outer surface may prove difficult. The foil-gage, panel-to-panel seals must carry significant aerodynamic pressure at elevated temperature without significant leakage or other failure (e.g. flutter) under a variety of loadings for the life of the TPS. Failure of a seal could have serious consequences. Gaps between panels and around the stand-off brackets allow direct radiation from the hot outer surface to the protected vehicle substructure. For the relatively brief heating pulse of the X-33 this radiation may not be significant. However, for the longer heating pulse of an RLV the radiation may overheat the substructure. Carrying aerodynamic pressures on the outer surface of the TPS means that creep of the outer honeycomb sandwich may limit the maximum use temperature.

The SA/HC TPS (figure 3) has seals and attachments on the cooler side of the panel, enabling a much wider choice of seal and attachment materials and configurations. The vented design greatly reduces the pressure loading and associated material creep at elevated temperature, thereby providing the potential for higher use temperatures. However, the bi-material (Inconel and titanium) configuration is more complicated and costly to fabricate. The rigid, beaded side walls require unique tooling for each thickness and curvature. The stiff sides also couple the thermal deformation of the outer Inconel honeycomb and inner titanium honeycomb, exacerbating thermal bowing.

Developing metallic TPS to meet the challenging goals of the RLV will require improved concepts that build on the strengths of current designs while avoiding their drawbacks. The experience being gained under current efforts provides a basis for conceiving improved metallic TPS concepts for RLV.

3. TECHNOLOGY DEVELOPMENT FOR METALLIC TPS

The two metallic TPS concepts shown in figures 3 and 4 share several common features. The outer surface of each concept is comprised of a high-temperature, foil-gage, metallic honeycomb sandwich. Materials and fabrication techniques are similar. Both concepts have low density, internal, non-load bearing insulation. Tests and analyses of the response of foil-gage metallic honeycomb sandwich to the anticipated RLV environment are therefore applicable to both of these concepts and to future metallic TPS. Efforts to characterize and improve low density, non-load bearing insulation will benefit a wide range of current and future TPS concepts. However, specific panel level tests are also required for each TPS concept to verify its thermal and structural performance.

This section of the paper briefly highlights some of the recent metallic TPS development efforts. Some of this work was completed under Phase I of the X-33 program, and some is being performed under Phase II.

3.1 Testing and Analysis for Durability

The TPS for a vehicle such as the RLV may encounter low speed impacts from tool drop, handling, launch debris and runway debris; hypervelocity impact from orbital debris or micrometeoroids; and erosion from flying at high speeds through rain. Coupons of foil-gage metallic honeycomb representative of the outer surface of metallic TPS were subjected to low speed impacts, hypervelocity impacts and rain erosion. Damaged specimens were then subjected to hot gas flow in an arcjet. Inconel 617 and titanium 6Al-4V specimens with several facesheet thicknesses and core geometries were tested. In addition, an analytical model of a superalloy honeycomb TPS panel being impacted by a hypervelocity projectile is being developed. This model will be used to improve the resistance of metallic TPS to hypervelocity impacts in the most mass efficient manner.

3.1.1 Low-speed impact tests

The susceptibility of TPS to low-speed impact damage from handling, tool drop, and low-speed debris impact during launch and landing will greatly affect the amount of refurbishment required between flights. If a TPS can sustain a low-speed impact with minimal damage so that immediate refurbishment is not required, maintenance time can be greatly reduced.

Low-speed impact tests were performed (Ref. 9) on a variety of Inconel 617 and titanium honeycomb sandwich specimens using the low-speed impact facility at NASA LaRC (figure 5). The facility features a dropped impactor which is instrumented to measure the impact force profile. Interchangeable impact heads provide variable impact radii. A knife-edge support fixture approximates simply supported boundary conditions for the 10-cm-square impact specimens.

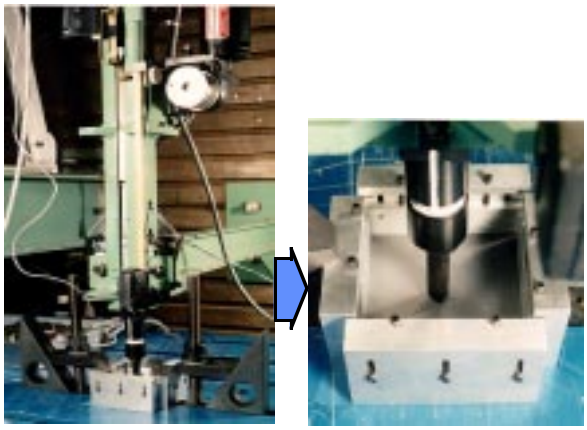

Figure 5. Low-speed impact test apparatus.

Inconel 617 honeycomb sandwich specimens with facesheets from 0.06- to 0.25-mm thick, and titanium honeycomb sandwich specimens with facesheets from 0.08- to 0.41-mm thick were tested (Ref. 9). Impact energies ranged from 1.4 to 14 N-m, and impact diameters ranged from 0.6 to 10.2 cm. The objectives of the testing were to characterize the material response to low-speed impact and to develop a method to design for low speed impact resistance. An example of the test results and characterization method is illustrated in figure 6. A specimen impacted by a 0.6-cm-diameter impactor at an energy of 2.8 N-m produced the force profile shown. The peaks in the force profile correspond to the impact head encountering the two facesheets of the honeycomb sandwich. Sharp drops in the force profile near the force peaks correspond to the impactor breaking through the facesheet. The impact force profile can be integrated and manipulated to calculate the impact energy as a function of time during the impact. By determining the impact energy at the time of facesheet cracking, a threshold value was calculated. Plotting the resultant threshold values as a function of facesheet thickness produces the chart on the lower left of figure 6 which can be used for design purposes.

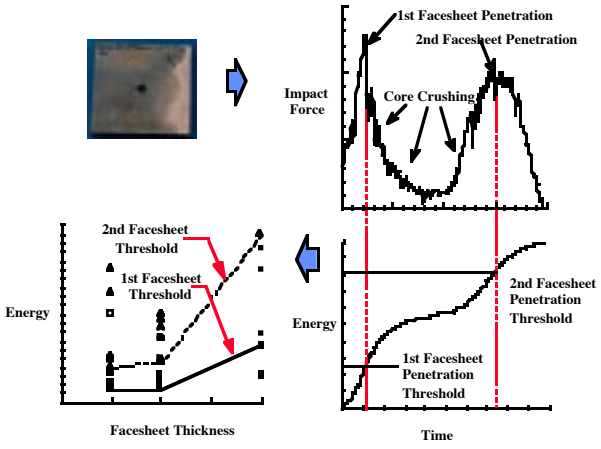

Figure 6. Low speed impact characterization of Inconel honeycomb sandwich.

Figure 7. Inconel 617 low-speed impact specimen after arcjet exposure.

Three preoxidized Inconel 617 and titanium specimens were impacted by 0.6-, 1.6- and 10.2-cm-diameter impact heads, and subsequently exposed to arcjet flow in the Panel Test Facility (PTF) at NASA Ames Research Center. One of the specimens is shown in figure 7. The Inconel and titanium specimens were exposed to 13 minutes of flow at 1260K and 810K respectively. Some of the Inconel specimens experienced a spallation of some of the oxidation on the outer surface. The reason for this loss of oxide layer is not totally understood, but it appears to be related to a pattern of overheating on the specimen surface. The arcjet flow did not appear to enlarge the damaged area on the specimens.

3.1.2 Rain erosion tests

The rain erosion resistance of the TPS is one of the key RLV operability issues. If the TPS can survive rain impact, the vehicle's economic viability and performance will be improved because it will able to operate in adverse weather conditions.

Two different types of rain erosion tests were performed on the honeycomb sandwich specimens. Small, 2.5-cm-diameter specimens were tested in the rotation arm facility at the University of Dayton. Larger, 10 cm by 15 cm and 10 cm by 10 cm specimens were flight tested on an F-15 aircraft.

Both preoxidized and unoxidized specimens were tested at a number of speeds and angles of attack in the rotating arm facility. Circular, 2.5-cm-diameter specimens of both Inconel 617 and titanium honeycomb sandwich with 0.13-mm-thick facesheets and 6.4-mm-deep core with 4.8 mm-diameter cells made from 0.04-mm-thick foil were tested at 30°, 60°, and 90° angles of attack at speeds of 63, 183 and 290 m/s for 90 and 180 seconds. The 2-mm-diameter water drops simulated a rainfall rate of 2.5 cm/hour. The unoxidized Inconel 617 specimens, after exposure to rain erosion, are shown in figure 8. The specimens exhibited no significant damage at 30° angle of attack or at 63 m/s. At 60° and 90° angle of attack for velocities of 183 and 291 m/s, the specimens were severely damaged with facesheet

cracking. Similar results were obtained for the titanium specimens, except that the failure mode was a breaking of the facesheet to core bond rather than the facesheet cracking observed in the Inconel specimens. Preoxidized and unoxidized Inconel 617 specimens exhibited similar behavior, however the preoxidized titanium specimens exhibited slightly more facesheet-to-core bond failures than the unoxidized specimens.

Both the preoxidized Inconel 617 and titanium specimens were subjected to arcjet testing in the Panel Test Facility (PTF) at NASA Ames following the rain erosion tests. The Inconel 617 specimens were tested at approximately 1260K and the titanium specimens were tested at 810K for 13 minutes. The oxide layers on both materials changed appearance but the extent of physical damage did not appear to change. The core-to-facesheet joints in the titanium specimens, however, may have been embrittled.

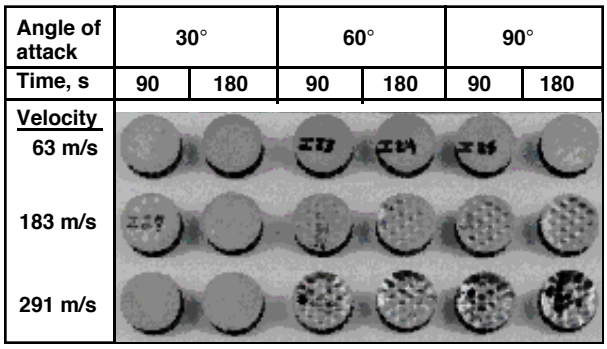

Figure 8. Inconel 617 honeycomb coupons tested in rotating arm rain erosion facility.

Rain erosion flight tests on an F-15 aircraft were conducted by Rockwell International (now part of the Boeing Company) at NASA Dryden. A special fixture was designed to suspend TPS samples beneath an F-15 aircraft as shown in figure 9. The fixture provided for eight rows of TPS samples. Each row had a sample at 0°, 10° and 20° angle of attack. Therefore eight TPS samples could each be tested at three different angles of attack. The primary purpose of the tests was to evaluate the rain erosion resistance of rigid ceramic tiles and flexible blankets. However, preoxidized Inconel 617 and titanium honeycomb sandwich samples were also tested. The metallic specimens were flown at a variety of conditions from light mist to very heavy rain at speeds up to 260 m/s over the course of five test flights. The 0° and 10° specimens were unchanged in appearance. The 20° specimens had slight intracell dimpling of the facesheets, which was surprising since the rotating arm specimens had exhibited no dimpling at 30° angle of attack at 290 m/s. The dimpling may be due to the occasional impact with rain drops much larger than 2-mm-diameter encountered in the much longer exposure times in real rainfall during the flight tests. The damage that was observed was for a much more severe environment than that expected for acreage areas of the RLV.

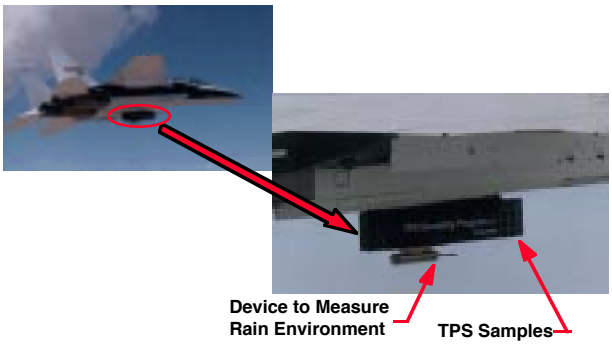

Figure 9. Rain erosion flight tests on an F-15 aircraft.

3.1.3 Hypervelocity impact tests

The threat of hypervelocity impact from micrometeorites, and especially man-made space debris, is an increasing concern for spacecraft and RLV's. Because the TPS will cover most of the external surface of the RLV, it is important to understand how well the TPS can withstand hypervelocity impacts and how well it can protect the underlying structure from damage.

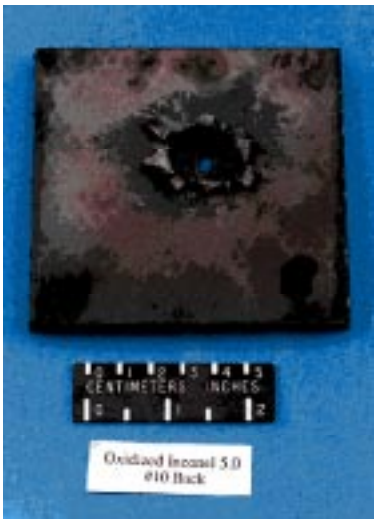

Figure 10. Inner facesheet of an oxidized Inconel 617 honeycomb sandwich coupon after hypervelocity impact.

More than 30 metallic TPS specimens were tested at the light-gas gun facility at NASA Marshall Space Flight Center (MSFC). A special fixture was developed to hold honeycomb sandwich coupons, internal insulation, a titanium foil or honeycomb coupon, and substructure panel to simulate a SA/HC TPS panel attached to a substructure. Aluminum spheres, with diameters of 3.2 to 6.4 mm, were fired at the specimens at 7 km/sec. The baseline Inconel 617 honeycomb sandwich with 0.13-mm-thick facesheets was able to break up the 3.2-mm sphere so that the 2.5-mm-

thick aluminum substructure was only slightly pitted. However, the 6.4 mm-diameter sphere produced a large hole in the aluminum substructure after penetrating the Inconel honeycomb sandwich, internal insulation, and 0.08-mm-thick titanium back surface. Figure 10 shows typical damage to the outer honeycomb sandwich. A small hole is produced in the outer surface, but the particle begins to break up and creates a much larger hole on the inner surface of the sandwich. Several Inconel 617 and titanium panels subject to hypervelocity impacts were subsequently tested in the PTF arcjet at NASA Ames. The arcjet flow appeared to cause some changes to the oxide layer on the outer surface, but did not enlarge the damaged area.

3.1.4 Hypervelocity impact analysis

Hypervelocity impact analysis (Ref. 10) is being pursued to develop a method for designing more impact resistant metallic TPS. A simplified, axisymmetric model of the impact of a particle normal to the center region of a TPS panel, away from any edges or fasteners, was developed using the CTH hydrodynamic code (Ref. 11). A sketch of the idealized problem and the corresponding axisymmetric model is shown in Figure 11. A configuration, from the test program previously described, was selected for analysis. The impacting particle was a 4.76 mm diameter aluminum sphere with an impact velocity of 7.1 km/s. A titanium honeycomb sandwich was modeled because a titanium material model was available in the hydrodynamics code used for analysis.

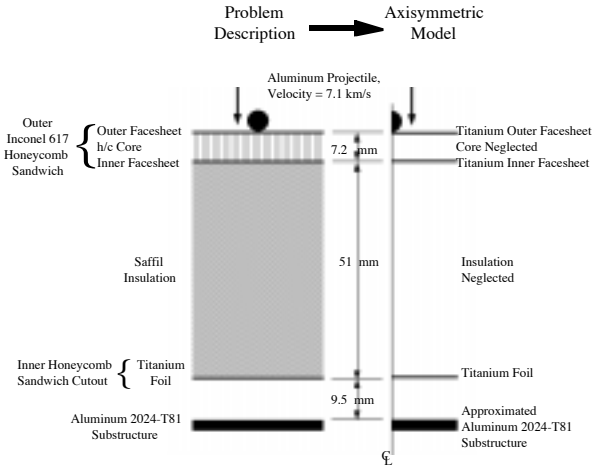

Figure 11. Description of hypervelocity impact problem and resulting axisymmetric model.

Two axisymmetric models of metallic TPS are discussed in this paper. The model shown in figure 11 accounts for the outer facesheet, inner facesheet, titanium foil, and substructure, neglecting the honeycomb core and Saffil insulation. Results for a similar model, which neglects the titanium foil, are also presented. Details of the material models, discretization of the models and corresponding computer run times are presented in reference 10.

Figure 12 shows the progression of the expanding impact debris cloud predicted by the axisymmetric model. The melting point temperature (930K) and vaporization temperature (2300K) of aluminum are listed on the figure and the shading bands roughly correspond to the solid, liquid, and vapor phases of the material. The outer foil layer, despite being much thinner than the projectile diameter, has shocked the projectile at 1.0 μsec after impact causing spalling to occur. Spalling is a tensile failure resulting from the reflection of compressive waves at free surfaces. The debris cloud is composed mostly of solid particles at this point. Upon impact with the inner facesheet, the debris cloud was further shocked. The leading edge of the debris assumes a vaporous state, with solid debris located at the center. As it progresses through the void between the inner facesheet and the titanium foil, the debris cloud expands radially. The debris cloud penetrated the titanium foil at 9.34 μsec after impact and proceeded to penetrate the substructure.

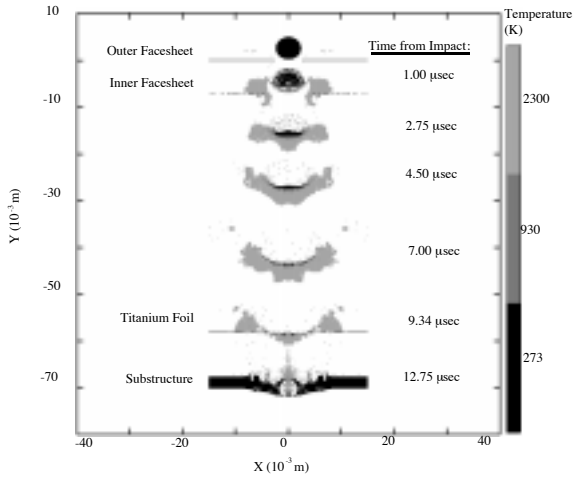

Figure 12. Time elapsed view of TPS penetration predicted by axisymmetric model with titanium foil.

Table 1 compares hole diameters of the outer facesheet, inner facesheet, titanium foil, and substructure predicted by the two analytical models with experimentally measured holes. The range of hole sizes in the table is due to the irregular shape of the experimental holes and the distribution of fragment holes in the axisymmetric analysis. The hypervelocity impact experiment resulted in substructure penetration. Petalling occurred on the inner facesheet, accounting for the majority of the recorded hole size. The titanium foil layer, in addition to having a hole form in it, developed an 11 cm tear. The substructure was visibly bulged outward by approximately 0.35 cm in the center of the plate. In addition, craters produced by fragments surrounded the hole. A second substructure hole

was produced by a fragment of the projectile. Computed hole sizes for the outer facesheet layer are smaller than the experimental hole size. A large discrepancy is also seen between experimental and computational hole sizes for the inner facesheet layer. This may be due to the inability of axisymmetric models to simulate the tearing and petalling seen experimentally. In addition, CTH does not have the capability to accurately model phenomena that occur well after the initial impact when pressures drop to a lower level. Hole sizes in the titanium foil layer suffer from the same limitations. However, hole sizes in the thicker substructure will be modeled more accurately, because it is not as susceptible to tearing and petalling. As seen in Table 1, predicted hole sizes in the substructure are similar to experimental hole size. Hole sizes are predicted to be larger when the titanium foil is neglected.

Table 1: Hole size comparison

	Outer facesheet (cm)	Inner facesheet (cm)	Titanium foil (cm)	Sub-structure (cm)
Experimental Results	0.81	3.38 - 4.88	2.54	0.43 - 0.94
Model with titanium foil	0.53	0.9 - 1.44	1.36 - 2.4	1.09 - 1.46
Model without titanium foil	0.53	0.9 - 1.44	N/A	1.47 - 2.13

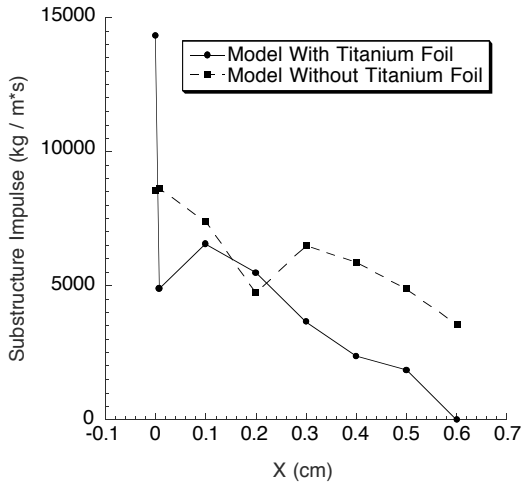

Figure 13. Comparison of peak substructure impulses generated with and without a titanium foil layer.

A comparison between the substructure impulses generated computationally is given in figure 13. Substructure impulse measures the transfer of momentum from the debris cloud to the substructure, and is therefore a good measure of the momentum distribution in the debris cloud and its damage potential to the substructure. In general, the peak impulse is substantially larger without the titanium foil layer, suggesting that this layer, despite its small thickness, has a large influence on the debris cloud damage potential. These analytical models will be used to efficiently improve the hypervelocity impact resistance of metallic TPS.

3.2 Panel Tests

Tests of TPS panels and panel arrays are an important part of a TPS development program. Panels were subjected to simulated flight loading, including thermal, pressure, acoustic, dynamic and hot gas environments. The development plan, including TPS panel testing, for the X-33 metallic TPS is described in reference 8. One of the most critical tests for the X-33 metallic TPS is the hot gas flow test described in reference 13. The hot gas flow test of an array of X-33 metallic TPS panels is critical to prove the performance of the panel-to-panel seals.

A number of superalloy honeycomb TPS panel tests are described in reference 7. A two-panel array was tested in a thermal vacuum facility with carefully controlled thermal boundary conditions to characterize the thermal performance and thermal deformations of the TPS panels. A four-panel array was tested in arcjet flow to determine the response to the hot gas environment. The four-panel array was subsequently tested in an acoustic environment to simulate the engine acoustic loads.

The preoxidized, four-panel array, shown in figure 14 prior to testing, was tested in the Interaction Heating Facility (IHF) arcjet at NASA Ames. The four TPS panels were mounted to a representative composite fluted-core structural panel using bonded-on threaded studs. Thermocouples were located at several locations down the sides of the panels, in the gaps, and on the substructure. The array was tested in two different arcjet runs. The first test was a check out test lasting less than five minutes and the second test lasted 11 minutes with a maximum surface temperature of approximately 1290K. The composite substructure reached a peak temperature of just under the 450K allowable temperature. Visual observations and infrared camera images during the test did not indicate a nonuniform surface heating variation which would be expected to result from significant thermal bowing of the panels. This was surprising because earlier tests of similar panels in NASA LaRC's 8 Foot High Temperature tunnel had resulted in heating variations associated with thermal bowing of the panels. The TPS panels survived the two arcjet tests with no sign of any damage as shown in figure 15. The surface oxidation appeared to transition from a greenish chromium oxide toward a dark gray nickel oxide. Temperature measurements taken during the tests gave no indication of hot gas flow in the gaps between panels.

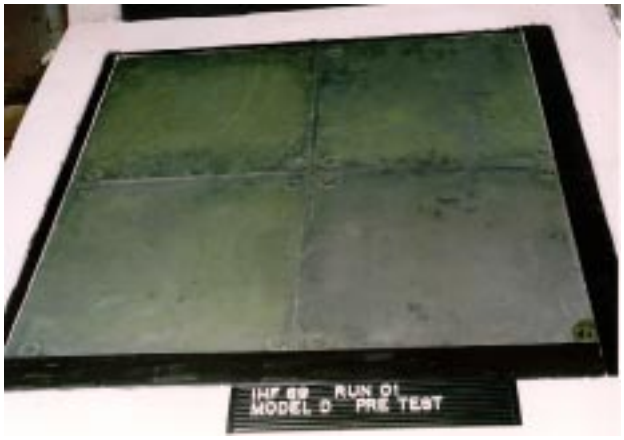

Figure 14. SA/HC TPS four-panel array before arcjet testing.

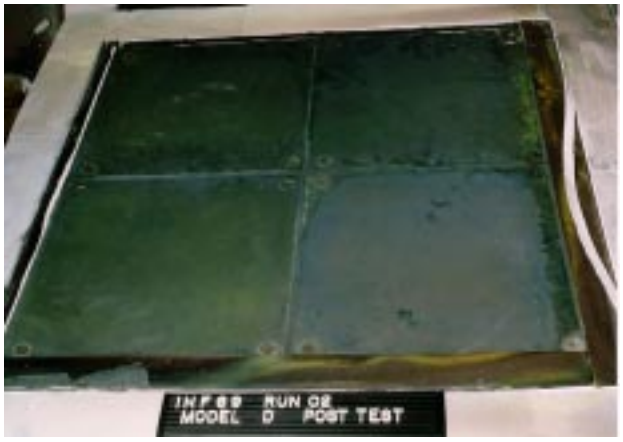

Figure 15. SA/HC TPS four-panel array after two arcjet tests.

3.3 Insulation Characterization and Development

The present TPS insulation concepts being investigated include low-density, high-temperature, fibrous insulation and multilayer insulation. The multilayer insulation consists of thin ceramic composite foils with high reflectance coating separated by fibrous insulation spacers. One of the multilayer insulations being investigated is the internal multiscreen insulation (IMI) described in reference 14. Efforts are being made at NASA LaRC for better characterization of the thermal performance of high temperature insulation. One activity consists of measuring the effective thermal conductivity of candidate insulations using steady-state experiments subject to varying air pressures and large temperature gradients representative of reentry conditions. Another activity is comprised of developing a complete numerical thermal model of the complex heat transfer through the insulation, and using experimental techniques to estimate some of the parameters needed in the formulation and validation of the numerical models. The validated models can then be used to optimize combinations of insulations for specific reentry profiles.

The heat transfer through candidate insulations is a complex, nonlinear problem involving combined modes of heat transfer: solid conduction through fibers, gas conduction and natural convection in the space between fibers, and radiation through participating media which includes absorption, scattering and emission of radiant energy by the fibers. For multilayer insulations, radiation also takes place through reflection and emission of energy by reflective foils.

The operational envelope of a typical metallic TPS for RLV reentry is complex: the environmental pressure varies from 10^{-2} to 760 torr, the hot surface of the TPS reaches temperatures as high as 1000°C, while the substructure protected by the TPS is limited to 200°C. Therefore, the insulation is exposed to varying pressure, high temperatures, and is required to maintain large temperature gradients (800°C) across its thickness. The relative contributions of the different heat transfer modes vary during reentry due to the varying environmental conditions. Radiation becomes more dominant at high temperatures and with large temperature gradients while the contribution of gas conduction is minimal at low pressures and becomes more significant with increasing pressure.

The accepted technique for simplifying the analysis of the complex heat transfer through candidate TPS insulation material has been to use the measured effective thermal conductivity. The contributions of various modes of heat transfer are lumped into an effective thermal conductivity. The standard technique for measuring the effective thermal conductivity of insulation materials is the guarded hot plate method, but this technique requires measurements to be taken with small temperature gradients across the sample. Thermal analysis which models insulation with an effective thermal conductivity may not accurately simulate the performance of low density insulation with large temperature gradients, where radiation becomes a dominant mode of heat transfer.

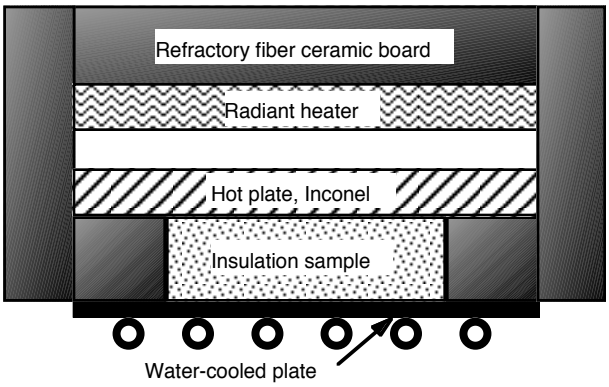

Figure 16. Schematic of the thermal conductivity apparatus.

A thermal conductivity apparatus was designed and constructed to provide effective thermal conductivity

measurements with samples subjected to large temperature gradients. A schematic of the apparatus is shown in figure 16. The apparatus was developed to follow the American Society of Testing and Materials (ASTM) standard C 201, consisting of a radiant heater, an Inconel septum plate and a water-cooled plate. A picture frame made of refractory fiber ceramic board was set on the water-cooled plate with the insulation sample to be tested placed inside the picture frame. The septum plate was then laid on top of the picture frame with the radiant heater placed approximately 3 cm above the septum plate. The standard sample size was 20 by 20 cm, and its thickness could vary from 1.3 to 5 cm. The entire assembly was enclosed in refractory fiber ceramic boards and placed in a vacuum chamber capable of providing pressures from 10^{-4} to 760 torr. The septum plate can be heated to 1000°C, while the water-cooled plate temperature can be maintained at temperatures between 15°C and 40°C. For a typical test, temperatures were measured at various locations on the septum and water-cooled plates using thermocouples, while the heat flux was measured at various locations on the water-cooled plate using thin film heat flux gages. The thermal conductivity was measured at various locations inside and outside the metered region (the central 10 by 10 cm region). This served two purposes: to verify one-dimensional heat transfer in the metered region and to provide an average thermal conductivity value.

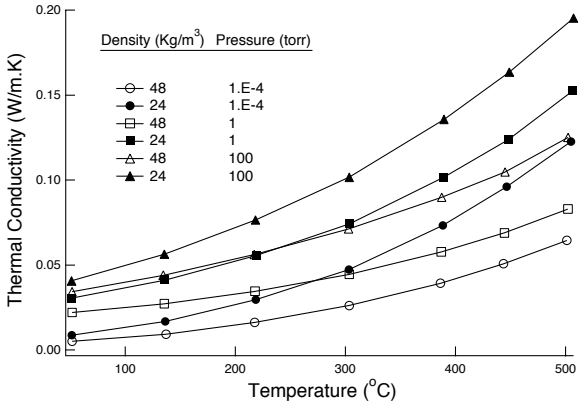

Figure 17. Variation of effective conductivity of saffil at various densities with mean temperature.

The effective conductivity of an insulation sample was calculated from Fourier's law using the measured heat flux, septum and water-cooled plate temperatures, and sample thickness. The uncertainty of the thermal conductivity measurements was estimated to be ±6%. Using this apparatus the thermal conductivity for a 2.5 cm thick fused silica board, a standard reference material used by the National Institute of Standards and Technology, was measured to be within 4% of published data. The measured effective thermal conductivity of saffil (alumina-based fibrous insulation) at nominal densities of 24 and 48 kg/m^3 as a function of mean temperature (average of hot and cold side temperatures) for three different pressures is shown in figure 17. The cold side was maintained at room temperature for all tests. The conductivity of saffil rises rapidly with temperature, indicating the dominant role of radiation heat transfer. Radiation is particularly important for the lower density saffil. The variations of conductivity with pressure indicate that gas conduction is also an important mode of heat transfer within the insulation.

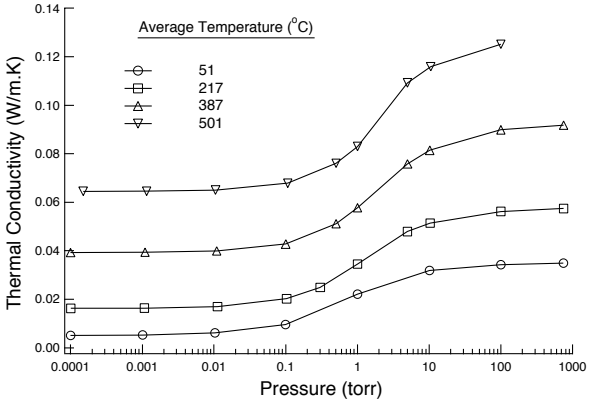

Figure 18. Variation of effective thermal conductivity of saffil (48 kg/m^3) with pressure.

The effective thermal conductivity of saffil at 48 kg/m^3 as a function of pressure for four different mean temperatures is shown in figure 18. Below 0.1 torr the conductivities are nearly constant with pressure, indicating that gas conduction is negligible. By comparing the conductivities at low pressure and at one atmosphere, the relative contributions of the two dominant modes of heat transfer, radiation and gas conduction, can be seen. At lower temperatures, gas conduction dominates, but at higher temperature, radiation dominates. Similar tests are planned for q-fiber (silica-based) and cerachrome (silica/alumina-based) fibrous insulations and two multilayer insulations.

4. MASS COMPARISON WITH OTHER TPS

To assess the mass competitiveness of metallic TPS, a study was conducted to compare the total system masses of a number of TPS concepts over a variety of heating conditions (Ref. 15). Thermal protection systems compared included concepts developed for the Space Shuttle Orbiter and systems proposed for RLV's. In this section, a brief description of the overall study and a summary of the results will be presented.

The study was conducted using a specially developed TPS analysis and sizing computer code. For this code, one-dimensional thermal models and mass models have been developed for a number of TPS concepts. Schematics of a metallic TPS concept and the corresponding 1-D analysis model are shown in figure 19. These models, which include contributions from coatings, adhesives, fasteners, and strain isolation pads, were then incorporated into a

transient thermal analysis and sizing computer code. The TPS sizing code uses a nonlinear, implicit, one-dimensional, transient, finite element solution technique to compute temperatures throughout the TPS and simple iterative algorithms to size the TPS. The TPS sizing code allows for rapid and accurate assessments of TPS requirements over a variety of vehicle heating and structural configurations.

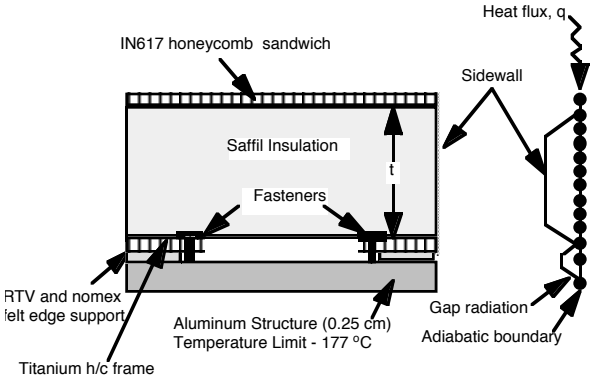

Figure 19. Schematic of a SA/HC TPS concept and the associated 1-D analysis model.

A simple structural arrangement consisting of TPS directly attached to a 0.25-cm-thick aluminum substructure was selected for the study. The temperature of the aluminum substructure was limited to a maximum of 177°C, and the required TPS thickness was sized to satisfy this constraint.

To generalize the results somewhat, reentry heating rate predictions for two single-stage reusable vehicles, the Access to Space (ATS) vehicle and a proposed Lockheed RLV, were used for the study. The reentry heating profiles used are shown in figure 20 along with a view of each vehicle configuration. While the peak heating values are similar for each vehicle, the shapes of the profiles are quite distinct. Linearly scaled values of both heating profiles were used for the mass comparisons of the various higher temperature TPS concepts.

Ten different TPS concepts were investigated in reference 15, but only four will be discussed in this paper: the current SA/HC TPS, an advanced metallic honeycomb TPS concept (AMHC), Tailorable Advanced Blanket Insulation (TABI), and Alumina Enhanced Thermal Barrier (AETB) tiles with a TUFI coating. The SA/HC TPS concept considered in this study uses lightweight saffil insulation contained in a metallic box and is shown schematically in figure 19. The advanced metallic TPS concept replaces the Inconel 617 components of the SA/HC with an ODS alloy which has a lower density and a potentially higher use temperature. In addition to some minor structural and fastening modifications, the AMHC concept employs more efficient multilayer insulation as compared to the SA/HC. The AMHC concept has not been designed or tested but represents an estimate of the performance gain an advanced metallic TPS design might obtain. TABI blankets, developed as an improvement to the AFRSI currently certified on the Space Shuttle Orbiter, are the latest advance in ceramic blanket TPS. However, neither of these blanket systems has been tested on the windward surface of an entry vehicle. Integrally woven corrugations provide higher strength, and these blankets are predicted to have a maximum operational temperature of 1200°C. The AETB ceramic tile with a TUFI coating was developed as an improvement to the LI900 tile used on the Space Shuttle Orbiter. The AETB tiles demonstrate higher strength, added durability, and have a maximum operational temperature of 1370°C. The AETB-8 tiles included in this study have a density of 128 kg/m^3.

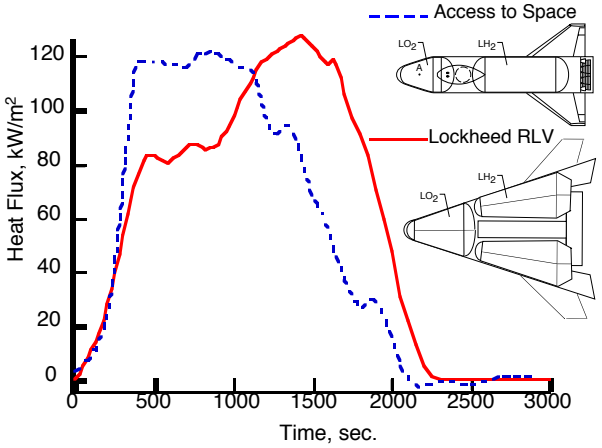

Figure 20. Reentry heating profiles used for the TPS mass comparison studies.

In the study of reference 15, masses of the various TPS concepts were compared for a variety of heat loads and substructural heat capacities. Although the heat flux histories for the two trajectories studied are considerably different (figure 20), TPS masses were nearly identical for the same total heat load. For this reason, only results from a single trajectory heating are shown. Results from one parametric study with the ATS reentry heating profile are shown in figure 21. TPS unit masses are plotted as a function of the total trajectory integrated heat load. The variations in total heat load were obtained by linearly scaling the applied heat fluxes for the Access to Space vehicle (figure 20) by factors ranging from 0.25 to 2.0. Unit mass data are not plotted for heat load cases where the maximum computed temperature exceeds the use temperature limit of the TPS concept.

Several trends can be seen in the data shown in figure 21. TABI blankets have the lowest mass at the lower heat loads, but also have the lowest useable heating level due to the low emissivity of TABI at higher temperatures. This low emissivity also reduces its mass advantage at higher heating rates. In addition, the viability of TABI blankets for application to windward surfaces remains to be proven.

The unit masses of the current SA/HC metallic TPS and the AETB-8 tiles are quite similar over the entire heating range. Ceramic tiles, including AETB-8, were the only TPS that could withstand the highest heating, highest temperature conditions studied. The advanced metallic TPS concept demonstrated the lowest mass over most of the heating range, and the benefits of using efficient multilayer insulation are most evident at the higher heat loads. While this advanced metallic TPS concept has not undergone rigorous design and testing, these results indicate that metallic TPS have the potential to be mass competitive with blanket TPS concepts at moderate heating levels and significantly lighter than ceramic tiles over their applicable temperature ranges.

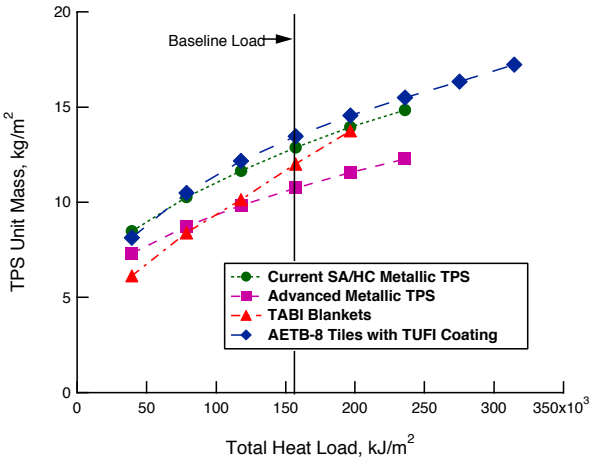

Figure 21. TPS unit mass as a function of total heat load using scaled heat loads from the Access to Space vehicle.

5. SUMMARY

With the advent of the X-33 program, metallic TPS are receiving renewed attention. NASA LaRC is building on its long history of metallic TPS development to help develop the technologies required for metallic TPS to meet the needs of future RLV's.

Two metallic TPS concepts of current interest, SA/HC TPS and X-33 metallic TPS share similar materials, honeycomb construction and fabrication techniques. However, the concepts are considerably different in configuration and operation. By building on the strengths and avoiding the weaknesses of these concepts, even better metallic TPS concepts can be developed to meet the ambitious RLV goals.

A range of foil-gage, metallic honeycomb coupons, representative of the outer surface of metallic TPS, were subjected to low-speed impact, hypervelocity impact and rain erosion. Some of the damaged specimens were subsequently exposed to arcjet flow. The resulting data provided some of the information needed to design metallic TPS for required levels of durability.

Analytical models are being developed for hypervelocity impact on metallic TPS. Axisymmetric models for a simplified configuration compare well with experiment. These models will be used to investigate the most mass efficient ways to improve hypervelocity impact resistance of metallic TPS.

A four-panel array of metallic panels (SA/HC) was tested in an arcjet at NASA Ames. The panels survived two tests in excellent condition with only a change in the appearance of the surface oxide layer. Measured temperatures indicated no evidence of significant hot gas flow in gaps between panels.

All metallic and refractory composite TPS will require lightweight, nonload-bearing insulation. Current experimental and analytical efforts are in progress to characterize existing insulations and develop improved insulations.

In a parametric sizing study, the weights of two metallic TPS concepts were compared with competing tile and blanket systems. Although the results varied somewhat over the range of parameters studied, the blankets were found to be lightest in most situations. Metallic panels and ceramic tiles were found to have comparable weight over most of the parameter ranges studied. Projected improvements in metallic TPS offer the potential for significant weight savings over current metallic and ceramic TPS concepts.

Metallic thermal protection systems are an attractive technology to help meet the ambitious goals of future space transportation systems. Improved concepts are being developed to meet the low-mass, durability and operability criteria required to dramatically reduce the cost of delivering payload to orbit.

6. REFERENCES

1. Baumgartner, R. I., 1998, VentureStar - A Revolutionary Space Transprotation Launch System, Presented at the Space Technology and Applications International Forum, 3rd Conference on Next Generation Launch Systems, Pp. 867-874.

2. Morris W, D., White, N. H., & Eberling, C. E. 1996, Analysis of Shuttle Orbiter Reliability and Maintainability Data for Conceptual Studies, AIAA 96-4245.

3. Bohon, H. L., Shideler, J. L., and Rummler, D. R., 1977, Radiative Metallic Thermal Protection Systems: A Status Report, *Journal of Spacecraft and Rockets*, Vol. 12, No. 10. Pp. 626-631, October 1977.

4. Shideler, J. L., Kelly, H. N., Avery, D. E., Blosser, M. L., & Adelman, H. M. 1982, Multiwall TPS—An Emerging

Concept, *Journal of Spacecraft and Rockets*, Vol. 19, No. 4, July-August 1982, Pp. 358-365

5. Gorton, M. P., Shideler, J. L., & Web, G. L., 1993, Static and Aerothermal Tests of a Superalloy Honeycomb Prepackaged Thermal Protection System, NASA TP 3257.

6. Cook, S. 1996, The X-33 Advanced Technology Demonstrator, AIAA-96-1195, AIAA Dynamics Specialists Conference, Salt Lake City, UT.

7. Blosser, M. L. 1997 Development of Metallic Thermal Protection Systems for the Reusable Launch Vehicle, NASA TM 110296.

8. Bouslog, S. & Strauss, B., 1998, Thermal Management Design for the X-33 Lifting Body, 3rd European Workshop on Thermal Protection Systems, ESTEC, The Netherlands.

9. Karr, K. L. 1996, Experimental Low Speed Impact Damage Threshold of a Metallic Thermal Protection System, Master's thesis. School of Engineering and Applied Science, George Washington University.

10. Poteet, C. C. 1998, Computational Study of Hypervelocity Impacts on Metallic Thermal Protection Systems, AIAA 8th International Space Planes and Hypersonic Systems and Technologies Conference, Norfolk, VA.

11. McGlaun, J. M., et. al., 1990, A Brief Description of the Three-Dimensional Shock Wave Physics Code CTH, Sandia National Laboratories, SAND89-0607.

12. Chhabildas, L. C., et. al., 1992, Whipple Bumper Shield Results and CTH Simulations at Velocities in Excess of 10 km/s, Sandia National Laboratories SAND91-2683.

13. Sawyer, J. W., Hodge, J., & Moore, B., 1998, Aero/Thermal Test of Metallic TPS for X-33 Reusable Launch Vehicle, 3rd European Workshop on Thermal Protection Systems, ESTEC, The Netherlands.

14. Muhlratzer, A., Handrick, K., & Weber, K. H., 1990, Hermes Thermal Protection System, Internal Multilayer Insulation (IMI), Federal Republic of Germany.

15. Myers, D., Martin, C., & Blosser, M., 1998, Parametric Weight Comparison of Advanced Metallic, Ceramic Tile, and Ceramic Blanket Thermal Protection Systems (TPS), NASA TM.